An Efficient Method for Improving the Dose-Volume-Based Optimization Plan Quality

CAIPING GUO[1,2,3], PENGCHENG ZHANG[1,2], ZHIGUO GUI[1,2], HUAZHONG SHU[4,5], (Senior Member, IEEE)

[1]National Key Laboratory for Electronic Measurement Technology, School of Information and Communication Engineering,
North University of China, Taiyuan 030051, China
[2]Key Laboratory of Instrumentation Science and Dynamic Measurement, School of Information and Communication Engineering,
North University of China, Taiyuan 030051, China
[3]Electronic Engineering Department, Taiyuan Institute of Technology, Taiyuan 030008, China
[4]Laboratory of Image Science and Technology, Southeast University, Nanjing 210096, China
[5]Centre de Recherche en Information Médicale Sino-Français, F-35042 Rennes, France

Corresponding authors: Zhiguo Gui (gzgtg@163.com); Huazhong Shu (shu.list@seu.edu.cn)

ABSTRACT Dose-volume (DV)-based objectives are widely used in most intensity-modulated radiation therapy treatment planning, because numerous DV endpoints have been utilized. In clinical practice, DV-based optimization (DVO) with uniform or random initial intensity distributions is utilized, but without considering the non-convexity of the DV objectives. To improve the quality of DVO radiotherapy plan and reduce the local minimum error generated by non-convexity of the DV objective, we proposed an efficient method (an organ-model-based optimization guiding DVO) to determine the initial intensity distributions for DVO. The new approach includes two steps. First, fluence map optimization, based on the organ model that adopts our proposed increasing objective function, to assure organ evaluation criteria Pareto surface, was performed. Second, DVO procedure was performed by using the initial intensity distributions determined in the first step. We demonstrated this technique in two kinds of clinical cases. DV histogram metrics were adopted as the criterion to evaluate the treatment plans. Compared with the conventional DVO plan with uniform initial intensity distributions, the improved DVO plan provided better protection of organ at risk (OAR); the planning target volume coverage was similar. Moreover, the improved DVO plan was better than the plan generated in the first step. The proposed method, with advantages in determining the initial intensity distributions, was highly efficient to improve DVO plans.

INDEX TERMS Dose-volume-based optimization (DVO), intensity-modulated radiation therapy (IMRT), generalized equivalent uniform dose (gEUD), gradient optimization algorithm, organ-model-based optimization.

I. INTRODUCTION

Intensity-modulated radiotherapy (IMRT) can achieve a good balance between the coverage and homogeneity of the planning target volume (PTV) while sparing the organs at risk (OARs) by modulating the intensity of beams [1]. Conventionally, the dose distribution in patients is mainly controlled by optimized physical and biological criteria.

Moreover, the biological criteria that consider both tissue structure and radiation response information were sometimes incorporated into the inverse planning process for IMRT [2], [3]. The practical use of optimized plans that are only based on radiobiological information should be carried out carefully, due to the uncertainties associated with the models and clinical experiences in adopting physical criteria, such as dose and dose-volume constraints [2]. Additionally, physical objectives are used to perform clinical inverse treatment planning, which is a current standard practice that evaluates treatment plans according to clinically acceptable dose and dose-volume indices. Among those physical-criteria-based radiotherapy optimization techniques, the most clinically relevant technique would be the one based on partial dose-volume constraints [4]. The maximal and minimal dose constraints can be treated as special forms of dose-volume constraints. Optimization methods based on

dose-volume (DV) are unlikely to change substantially in the near future, since abundant clinical experiences that utilize DV endpoints (i.e., above specific dose thresholds) have been accumulated, which can be directly incorporated into the optimization process [2]. For example, radiation-induced pneumonitis has been associated with the average dose of the lung, and the volume V_{20} [5]–[8], the latter of which can be considered to be a constraint in optimization model.

In commercial inverse planning systems, such as HELIOS (Varian Associates, Palo Alto, CA, USA) and Pinnacle (Philips, Milpitas, CA, USA), gradient-based optimization algorithms are used to solve the optimization problems, because those algorithms require fewer iterations to obtain a reasonable solution [9]. The major concern when using those algorithms is that the optimization iterations may get trapped in a local minimum. Deasy [10] reported that local minima did exist in dose-volume objective. Their observations suggested that the gradient-based optimization algorithms should be performed in a manner that avoids getting trapped in local minima. However, Wu and Mohan [11] reported that the local minima problem is not easily resolved, based on the results from several clinically relevant plans with random initial intensity distributions. Llacer *et al.* [12] confirmed Wu's conclusions via the same approach. They also claimed, however, that multiple local minima problem should not preclude the researchers from searching a clinically acceptable treatment plan based on gradient-based optimization algorithms. Rowbottom and Webb [13] reported that local minima were widely found and closely clustered together based on their approach of "configuration space analyses" for beamlet weights optimization. Jeraj *et al.* [14] reported that the local minimum errors were relatively small when using random or uniform initial intensity distributions. The above summary indicates that the DVO, which is solved by a gradient-based algorithm, can generate a clinically acceptable radiotherapy plan, although this plan may not be global optimal. The key solution when using DVO is to propose approaches to avoid (or at least reduce) local minimum error, and to improve the quality of the DVO plan, both of which are the purpose of this work.

Lacer *et al.* [12] reported that the probability of reaching the global minimum was determined by the initial intensity distributions. Zhang *et al.* [9] also reported that arbitrary selection of the initial value might lead to inferior solutions. In clinical practice, however, uniform or random intensity distributions are chosen as initial solutions in the radiotherapy optimization process [9], [11], [14]. With aim to improve the DVO plan quality, our study mainly focused on the selection of the initial intensity distributions.

Through introducing the concepts of dose-volume histogram (DVH) and dose distributions, Zarepisheh *et al.* [15] found that the organ evaluation criteria (OEC) Pareto surface(i.e., X_{OEC}) belonged to the DVH Pareto surface (i.e., X_{DVH}), if the sub-objective functions for each OAR and each target were the increasing function for OEC. The relationship can be mathematically expressed as $X_{OEC} \subset X_{DVH}$. Based on
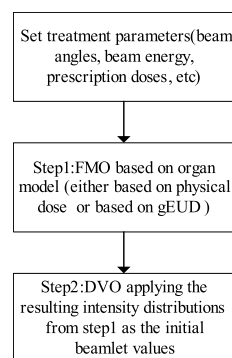
FIGURE 1. Outline of the new DVO method.

this theorem, we proposed a new approach to select the initial intensity distributions for DVO. In this approach, the initial intensity distributions are obtained by fluence map optimization (FMO) based on our improved organ-evaluation-criteria-based increasing optimization model. In the model, all voxels within a specific organ are tied together and treated equally.

As for optimization, according to $X_{OEC} \subset X_{DVH}$, we first optimized with the organ model, then proceeded with normal DVO optimization by using the fluence distributions from the first step as the initial intensity distributions.

The efficiency of the improved increasing functions was verified on a testing phantom TG119 and compared to that of the unimproved functions. The new DVO method was verified on two kinds of clinical cases, through comparison with the traditional DVO method and the organ-model-based optimization method used in the first step. The quality assessments of DVH metrics demonstrated that the new DVO method could potentially improve the commonly used technique of DVO.

In the following sections, we describe in details the materials and methods contained in the proposed method in Section II. We then show our experimental results in Section III, and finally discuss the results and future direction of research in Section IV.

II. MATERIALS AND METHODS
A. OVERALL OPTIMIZATION SCHEME
In this study, we assessed the sequential use of an organ-model-based optimization and the DVO to improve the DVO plan quality. As shown in Fig. 1, initial intensity distributions are first calculated in the search space X_{OEC} based on organ-model-based optimization with our proposed organ-based increasing objective function, which is shown in step1. Uniform initial intensity distributions were used for the organ-model-based optimization. In step 2, the DVO is carried out by using the initial intensity distributions obtained from step 1.

Two kinds of organ models, based on physical dose and gEUD, were adopted. The DVO, guided by the optimization with the organ model based on physical dose, was denoted as DBO+DVO. The DVO, guided by the optimization based

TABLE 1. Prescribed dose for the organ model based on physical dose.

Prostate	PTV	D_{mean}=78Gy
	Rectum	D_{max}=45Gy
	Bladder	D_{max}=50Gy
HN	PTV70	D_{mean}=70Gy
	PTV63	D_{mean}=63Gy
	PTV56	D_{mean}=56Gy
	Cord	D_{max}=30Gy
	Brainstem	D_{max}=40Gy
	L-Parotid	D_{max}=35Gy
	R-Parotid	D_{max}=35Gy

on gEUD was denoted as gEUDBO+DVO. All of the DBO, gEUDBO, and DVO belong to the fluence map optimization (FMO). In FMO, the weighted sum was used to build optimization model. Moreover, all of optimization problems were solved using gradient-based optimization algorithm (namely, L-BFGS) [16]. To avoid nonphysical solutions, the square roots of the beamlet weights were used as the optimized variables [17], and the maximum intensity limit was used to increase delivery efficiency [18].

B. IMPROVED ORGAN MODELS

In this section, we illustrate the original organ model based on physical dose sub-score or gEUD sub-score, and their improved organ-based increasing optimization models.

1) ORGAN MODEL BASED ON PHYSICAL DOSE

Three kinds of dose criteria can be adopted in FMO of IMRT: maximal dose criterion, minimal dose criterion, and mean dose criterion. In our organ model based on physical dose, the maximal dose sub-score was adopted to minimize the dose delivered to OAR, mean dose sub-score was adopted to guarantee the dose delivered to the PTV. A typical quadratic organ model based on physical dose for IMRT is illustrated as [15]

$$min_{x \geq 0} \sum_{\sigma \in C} \omega^{\sigma} \frac{1}{N_{\sigma}} \sum_{j \in \upsilon_{\sigma}} (w_j x - D_{max}^{\sigma})_+^2$$
$$+ \sum_{\sigma \in T} \omega^{\sigma} \frac{1}{N_{\sigma}} \sum_{j \in \upsilon_{\sigma}} (w_j x - D_{mean}^{\sigma})^2. \quad (1)$$

Here the function of $(\cdot)_+$ is equivalent to a step function, which produces a positive value if the actual dose, $w_j x$, exceeds the prescription dose D_{max}. Otherwise, there is no penalty. C and T are the set of tissues. Here C is the critical structures and T represents targets. The set of the voxels of the structures σ is denoted by υ_{σ}, and N_{σ} is the number of voxels belonging to the structure σ. ω^{σ} is the weight corresponding to the structure σ in the organ model. D_{max} and D_{mean} are the prescribed dose for critical structures and the prescription

mean dose for the target, respectively. w_j corresponding to voxel j, is the jth row of the dose deposition matrix, which is computed using the CERR pencil beam algorithm (QIB) with corrections for heterogeneities. x is the vector of beamlet weights (i.e., intensity distributions).

In problem (1), the semi-deviation penalty function for critical structure is not an increasing function for it does not differentiate the dose that is lower than the prescribed dose D_{max}. The theorem described in detail by Zarepisheh *et al.* [15] states that if objective function used to control C is an increasing function, and that controlling T is an increasing function of deviation to the prescribed dose in organ-model-based optimization, then we reach $X_{OEC} \subset X_{DVH}$. To guarantee Pareto optimality according to this theorem, the equation (2) was introduced to overcome this problem [15]. In equation (2), all doses lower than the prescribed dose are given a linear penalty function, and the doses higher than the prescription dose are given an extra quadratic dose penalty function, illustrated as follows:

$$min_{x \geq 0} \sum_{\sigma \in C} \omega^{\sigma} \frac{1}{N_{\sigma}} \sum_{j \in \upsilon_{\sigma}} (w_j x + (w_j x - D_{max}^{\sigma})_+^2)$$
$$+ \sum_{\sigma \in T} \omega^{\sigma} \frac{1}{N_{\sigma}} \sum_{j \in \upsilon_{\sigma}} (w_j x - D_{mean}^{\sigma})^2 \quad (2)$$

2) ORGAN MODEL BASED ON gEUD

The advantages of incorporating the *g*EUD concept into an optimization model have been widely verified by several researchers [2], [19]–[28]. Additionally, gEUD-based optimization has been incorporated into the Pinnacle system [29]. Previous work [23], [26] demonstrated the advantages of optimization based on a gEUD-based hybrid physical-biological model. A typical gEUD-based hybrid physical-biological optimization model can be described as:

$$min_{x \geq 0} \sum_{\sigma \in C} \omega^{\sigma} (gEUD(D) - gEUD_0)_+$$
$$+ \sum_{\sigma \in T} \omega^{\sigma} \frac{1}{N_{\sigma}} \sum_{j \in \upsilon_{\sigma}} (w_j x - D_{mean}^{\sigma})^2. \quad (3)$$

The gEUD-based sub-score also has the problem of semi-deviation penalty. In our experiments, according to the same method of constructing formula (2) to guarantee OEC Pareto, improved gEUD-based hybrid physical-biological model is

$$min_{x \geq 0} \sum_{\sigma \in C} \omega^{\sigma} (gEUD(D) + (gEUD(D) - gEUD_0)_+)$$
$$+ \sum_{\sigma \in T} \omega^{\sigma} \frac{1}{N_{\sigma}} \sum_{j \in \upsilon_{\sigma}} (w_j x - D_{mean}^{\sigma})^2. \quad (4)$$

Where gEUD is given by equation (5) [30] and gEUD_0 is the prescription dose.

$$gEUD(D) = (\frac{1}{N} \sum_{j=1}^{N} (D_j)^a)^{1/a} \quad (5)$$
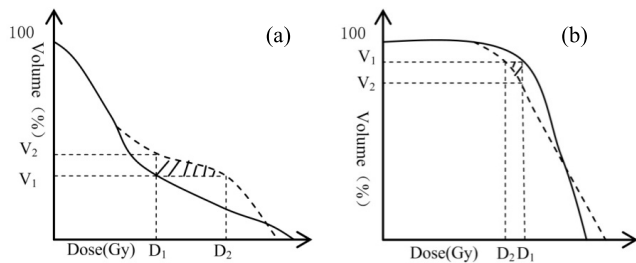
FIGURE 2. An illustration of (a) maximum and (b) minimum DV constraints. The dashed line is the current DVH, and the solid line is the objective DVH. The shaded parts denote the area in which the current DVH dissatisfies the DV constraint.

N is the number of voxels in the optimized structure, a is the tissue-specific parameter describing the dose-volume effect, and D_j is the dose to voxel j. For normal tissue and critical structures, a is defined as more than one, and function (5) is a convex function [19].

C. DOSE-VOLUME-BASED MODEL

Dose-volume constraints include both maximum and minimum dose-volume constraints. The maximum dose-volume constraint, which is representative of the volume receiving dose higher than D_1, in the case that V must be less than V_1 (mathematically expressed as V $(D > D_1) < V_1$). This constraint is usually used to control OAR and tissue structure, as well as PTV (Fig. 2.a). As for the minimum dose-volume constraint, which is specified as the volume receiving dose higher than D_1, in the case V that must be higher than V_1 (mathematically represented as V $(D > D_1) > V_1$), is applied to control low dose region of PTV (Fig. 2.b). The dose-volume-based sub-score has been described in detail by Wu *et al.* [31]. The sub-scores based on maximum and minimum dose-volume constraints are written as equation (6) and equation (7), respectively. Here N is the number of voxels in the optimized organ controlled by dose-volume constraints, D_2 is the dose received by volume V_1, and H is a step function. It is clear that the doses between D_1 and D_2, the shaded part in Fig. 2.a, are penalized in the equation (6) and the doses between D_2 and D_1, the shaded part in Fig. 2.b, are penalized in equation (7).

$$f_{maxdv} = \frac{1}{N} \sum_i H(D_i - D_1)H(D_2 - D_i)(D_i - D_1)^2 \quad (6)$$

$$f_{mindv} = \frac{1}{N} \sum_i H(D_i - D_2)H(D_1 - D_i)(D_i - D_1)^2 \quad (7)$$

The does-volume-based optimization model is

$$\min_{x \geq 0} \sum_{n \in T} \sum_{j=1}^n (\omega_1^j f_{\min dv}^j + \omega_2^j f_{\max dv}^j)$$

$$+ \sum_{m \in C} \sum_{i=1}^m \sum_{l=1}^k \omega_l^i f_{\max dv}^i \quad (8)$$

Where n is the number of targets, m is the number of OAR, and k is the number of dose-volume constraints for organ i.

It should be pointed out that, according to the theory of Pareto Optimality, we adjusted the weighting factors ω in all the optimization models by trial and error to ensure that the obtained solutions were on the PS (Pareto Surface). That is, for our optimized plans, if improvement in some evaluation criteria is only possible at the cost of another evaluation criterion.

D. TEST CASES

1) TG119 DATASET

TG119 [32] testing phantom that includes a C-shaped target (called "OuterTarget") and an OAR ("Core") that the target wraps around. The prescription dose for Core and OuterTarget were 0.4 Gy, and 1 Gy, respectively. Additionally, $a = 3$ was used for gEUD. Five equally spaced coplanar 6-MV photon beams were used for planning.

2) CLINICAL CASE

For prostate cancer cases, a PTV and two OARs (rectum and bladder) were considered in the optimization model. Table 1 lists the dose objectives for the optimization based on organ model based on physical dose. It required at least 99% of the PTV volume to receive 95% of the prescribed mean dose in the dose-based optimization model, and the D_{max} in rectum and bladder did not exceed their tolerance dose of 80Gy. Table 2 lists the radiobiological parameters of gEUD sub-score, which were part derived from the literature [20], [33], [34]. In the DVO, the dose distributions for the rectum and bladder were controlled by three maximum DV sub-scores, and PTV was controlled by a maximum DV sub-score and a minimum DV sub-score. Table 3 lists the DV objectives for the DVO. Five coplanar beams of 6-MV photons were used for all planning, with the gantry placed at 36°, 100°, 180°, 260°, and 324°.

For head and neck cancer (HN) cases, three PTVs (PTV70Gy, PTV63Gy, and PTV56Gy) and four critical structures (spinal cord, brainstem, L-Parotid, and R-Parotid) were incorporated into the optimization model. These PTVs were treated simultaneously with 70 Gy, 63 Gy, and 56 Gy, respectively. The prescribed doses for spinal cord and brainstem were 30 Gy and 40 Gy, respectively [31], while that for Parotids was 35 Gy [35]. In clinical practice, the tolerance dose for cord and brainstem should be less than 45Gy and 50Gy respectively, and mean dose for the Parotids should be less than 26Gy. The gEUD-based optimization parameters for head and neck cancer are also listed in Table 2. In the DVO, the dose distribution for each OAR was controlled by one maximum DV sub-score, and each PTV was controlled in the same manner as that for PTV in prostate cancer. DV objectives are listed in Table 3. Seven equally spaced coplanar 6-MV photons beams were used for planning.

TABLE 2. gEUD-based optimization parameters for prostate cancer and head and neck cancer.

Cases	Prostate		Head and neck			
Organs	Rectum	Bladder	Cord	Brainstem	L-Parotid	R-Parotid
$gEUD_0$(Gy)	35	35	35	40	20	20
a	8	8	7.4	4.6	5	5

TABLE 3. DV objectives for the DVO.

	PTV	$V_{74Gy}\geq99\%$	$V_{80Gy}=0$	
Prostate	Rectum	$V_{50Gy}\leq40\%$	$V_{65Gy}\leq25\%$	$V_{75Gy}\leq15\%$
	Bladder	$V_{65Gy}\leq35\%$	$V_{70Gy}\leq30\%$	$V_{75Gy}\leq16\%$
	PTV70	$V_{70Gy}\geq90\%$	$V_{77Gy}\leq2\%$	
	PTV63	$V_{63Gy}\geq90\%$	$V_{70Gy}\leq8\%$	
	PTV56	$V_{56Gy}\geq90\%$	$V_{59.9Gy}\leq10\%$	
HN	Cord	$V_{45Gy}=0$		
	Brainstem	$V_{50Gy}=0$		
	L-Parotid	$V_{50Gy}\leq20\%$		
	R-Parotid	$V_{50Gy}\leq20\%$		

E. EXPERIMENTAL ENVIRONMENT

The computational environment for Radiotherapy Research (CERR) version 4.0 [36] was used as our radiotherapy planning platform. The software provides a clinical data interface, dose calculation, and visualization function [37]. The dose deposited matrix was calculated by applying the standard pencil beam algorithm [38], and it is implemented by the CERR package. All experiments were performed by using an instrument equipped with a 32-bit OS, Windows 7, and an Intel (R) Core (TM) i3-4150 CPU with 4G RAM.

We used a Wilcoxon matched pairs signed ranks test with significant level of 5% to analyze the significant differences between the improved DVO plan and other plans.

III. RESULTS

Fig. 3.a and Fig. 3.b show the comparison results on the TG119 phantom from the improved increasing physical model (2) compared to the original non-increasing physical model (1), as well as the improved increasing gEUD-based hybrid model (4) compared to the original non-increasing hybrid model (3), respectively. From the comparative results of DVH metrics, the improved plan clearly shows better OAR sparing without reducing the PTV coverage and uniformity. In other words, better solutions, belonging to both X_{OEC} and X_{DVH}, can be gained when using increasing optimization model to perform organ-model-based radiotherapy optimization.

Next, we performed DVO guided by organ-model-based optimization by applying an increasing optimization model.
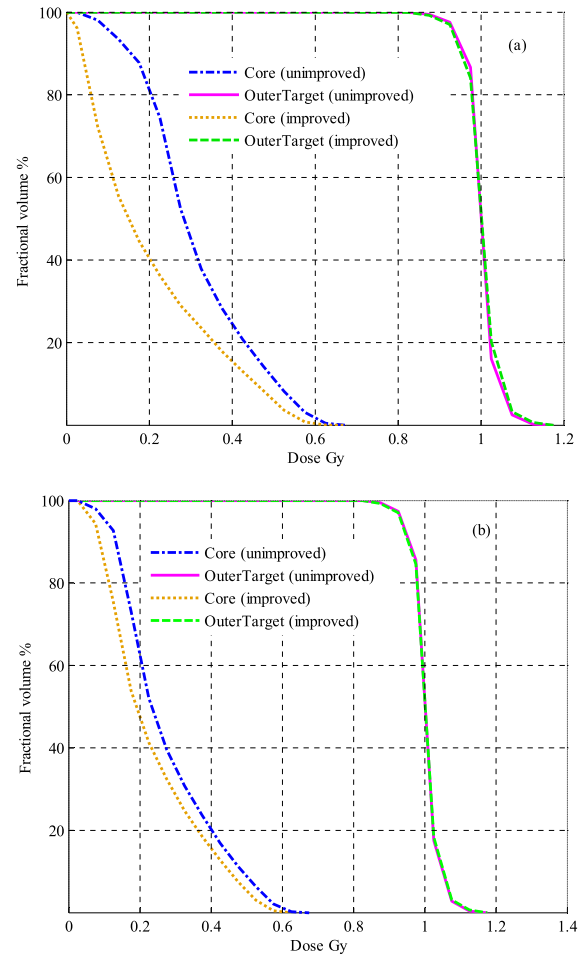
FIGURE 3. DVH comparison of treatment plans using different optimization models for optimization on TG119.

The physical dose sub-score weights and the gEUD sub-score weights for the prostate cases and the HN cases are listed in Table 4, Table 5, Table 6, and Table 7, respectively. Table 8 and Table 9 list the DV sub-score weights for prostate cancer cases and HN cancer cases, respectively. The optimized results, in terms of DVH metrics, were first compared with the results of the traditional DVO plan. To make a fair comparison, all the DVO plans (DVO, DBO+DVO, gEUDBO+DVO) for a specific cancer case use the same objective function and parameters (e.g., prescribed dose and weighting factors).

Fig. 4 shows the average DVH comparison between the traditional DVO plan (indicated by solid lines) and the improved

TABLE 4. Physical dose sub-score weights for five prostate cases.

	Bladder	Rectum	PTV
Case	ω_1	ω_2	ω_3
1	1	2	210
2	1	2	170
3	2	1	150
4	2	2	240
5	3	2	210

TABLE 5. gEUD sub-score weights for five prostate cases.

	Bladder	Rectum	PTV
Case	ω_1	ω_2	ω_3
1	20	15	380
2	20	15	300
3	4	2	450
4	3	3	650
5	12	4	108

TABLE 6. Physical dose sub-score weights for five HN cases.

	PTV70	PTV63	PTV56	Cord	Brainstem	L-Parotid	R-Parotid
Case	ω_1	ω_2	ω_3	ω_4	ω_5	ω_6	ω_7
1	18	8	2	1	1	1	1
2	78	75	15	20	1	1	1
3	75	75	15	20	1	1	2
4	25	30	25	10	1	2	1
5	25	30	25	10	2	2	1

TABLE 7. gEUD sub-score weights for five HN cases.

	PTV70	PTV63	PTV56	Cord	Brainstem	L-Parotid	R-Parotid
Case	ω_1	ω_2	ω_3	ω_4	ω_5	ω_6	ω_7
1	20	36	14	2	1	2	1
2	43	43	20	11	1	59	6
3	40	40	18	10	2	55	5
4	32	32	22	2	2	15	8
5	32	32	22	3	17	25	9

TABLE 8. DV sub-score weights for five prostate cases.

	Bladder			Rectum			PTV	
Case	ω_1	ω_2	ω_3	ω_4	ω_5	ω_6	ω_7	ω_8
1	1	1	4	2	3	3	84	68
2	1	1	4	2	3	3	39	43
3	7	4	2	1	3	3	150	61
4	4	5	10	1	2	2	71	49
5	5	3	2	2	2	2	220	90

DVO plan (indicated by dotted lines). The dotted lines in Fig. 4.a–4.b respectively show the average DVH resulting from DBO+DVO and gEUDBO+DVO for five prostate cancer cases. The dotted lines in Fig. 4.c–4.d show the average results based on DBO+DVO and gEUDBO+DVO for five HN cases, respectively. To make clear and detail comparisons, Table 10 and Table 11 show some average clinical metrics for the two types of cancer cases corresponding to the DVH endpoint values in Fig. 4, The DVH endpoint value with significant difference (DVO vs. DBO+DVO, DVO vs. gEUDBO+DVO) is shown in bold.

Fig. 4.a shows the average results of plans based on DVO and DBO+DVO for five cases of prostate cancer. Table 10 clearly shows that the PTV coverage is similar when comparing the DVH. The homogeneity (HI: $p > 0.05$), which is defined as the ratio of the minimum dose delivered to the volume 5% of the PTV to the minimum dose delivered to the volume 95% of the PTV [39], remains the same. In the DBO+DVO plan, the clinically relevant DV constraints in Table 12 [40] for the rectum are obviously reduced with significant differences except V_{75} ($p > 0.05$). The improvement percentages are V_{50} (11.32%), V_{60} (8.59%), V_{65} (6.52%), V_{70} (3.9%), and V_{75} (1.19%), respectively. The bladder V_{65}, V_{70} and V_{75} are improved by 5.74%, 2.88%, and 2.11%, respectively. In the DVO plan and the DBO+DVO plan, the maximum dose, not only to rectum but also to bladder, remains comparable. Fig.4.b illustrates the comparison between the DVO plan and gEUD+DVO plan for the prostate cancer cases. The PTV improvement is similar to that in Fig.4a. Rectal V_{50}, V_{60}, V_{65}, V_{70}, and V_{75} as well as bladder V_{65}, V_{70}, and V_{75} were improved by 7.64%, 5.87%, 3.31%, 3.01%, 2.08%, 6.47%, 3.78%, and 2.02%, respectively.

Similarly, the same comparisons were performed in five HN cancer cases. Fig. 4.c compares the average DVHs for the DVO plan and the DBO+DVO plan. It clearly demonstrates significant improvement for both all OARs and PTV high doses, whereas slightly under-dosing of PTV70. According to Table 11, the PTV63V (67.4 Gy), PTV56V (56 Gy), cord and brainstem maximum doses, and the L-Parotid and R-Parotid mean doses were improved by 20.97%, 0.88%, 12.93%, 7.33%, 8.61%, and 8.92%, respectively. The improvements in cord and brainstem maximum doses are of great significance to clinical practice, because of their serial nature, despite the fact that the doses delivered to them are already below the tolerance values. However, there is no reason why such a plan, which reduces the dose to OARs at no or less cost to the target coverage, should not be implemented. Additionally, reductions in the mean dose for the L-Parotid and R-Parotid are valuable for protecting them since they are parallel organs, indicating that their probability of tissue complications is determined by the mean dose. Fig. 4.d illustrates the average optimization results of plans based on DVO and gEUD+DVO. The PTV63V (67.4 Gy), PTV56V (59.9 Gy),
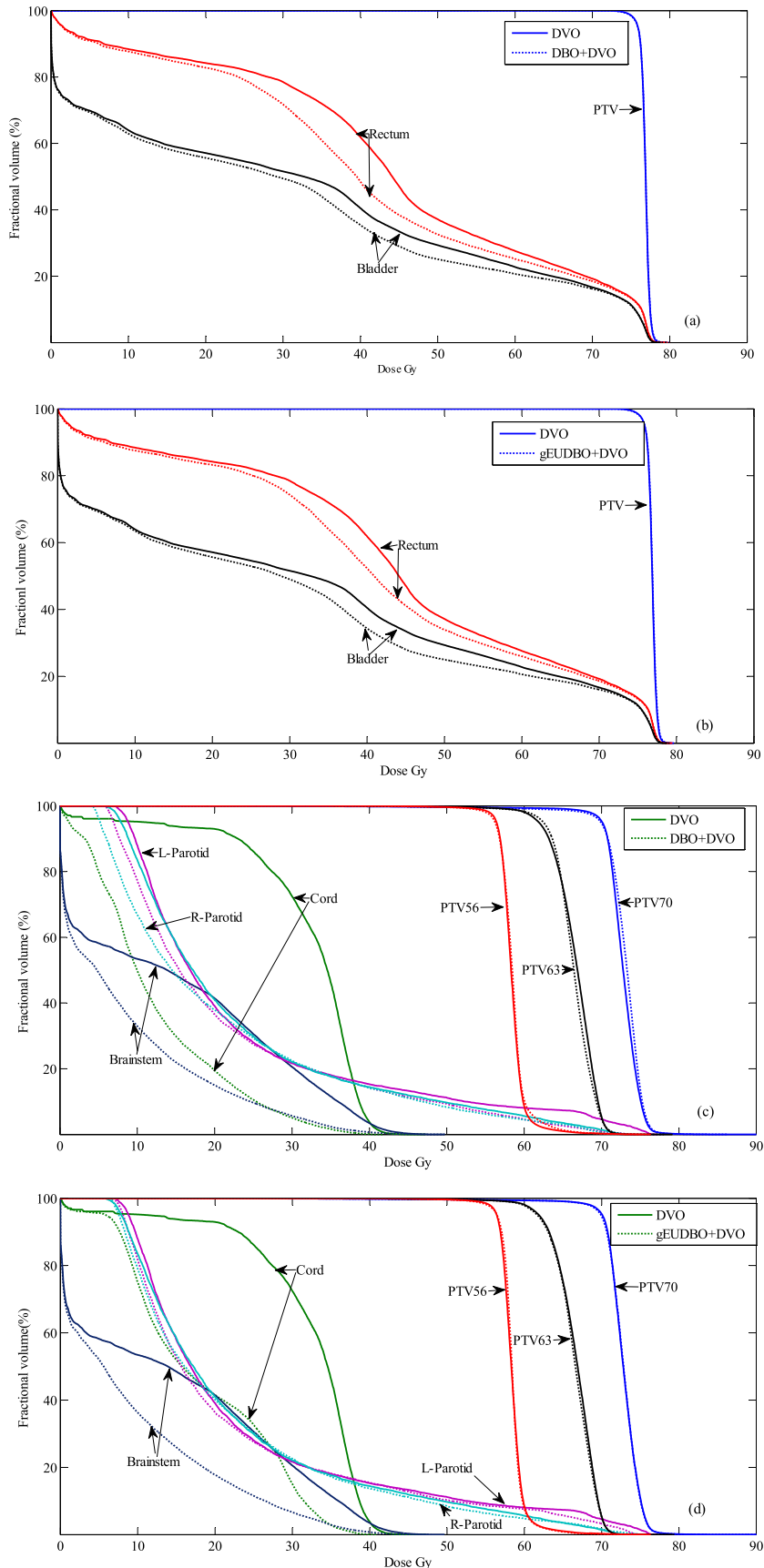
FIGURE 4. Average DVH comparisons of treatment plans. Dotted line: traditional DVO; Solid line: improved DVO.

TABLE 9. DV sub-score weights for five HN cases.

	PTV70		PTV63		PTV56		Cord	Brainstem	R-Parotid	L-Parotid
Case	ω_1	ω_2	ω_3	ω_4	ω_5	ω_6	ω_7	ω_8	ω_9	ω_{10}
1	20	15	76	37	14	13	3	2	20	8
2	16	34	3	27	3	19	10	1	2	1
3	19	20	30	42	25	17	3	2	18	6
4	16	34	3	27	3	19	10	1	2	1
5	16	13	3	27	3	19	10	1	12	80
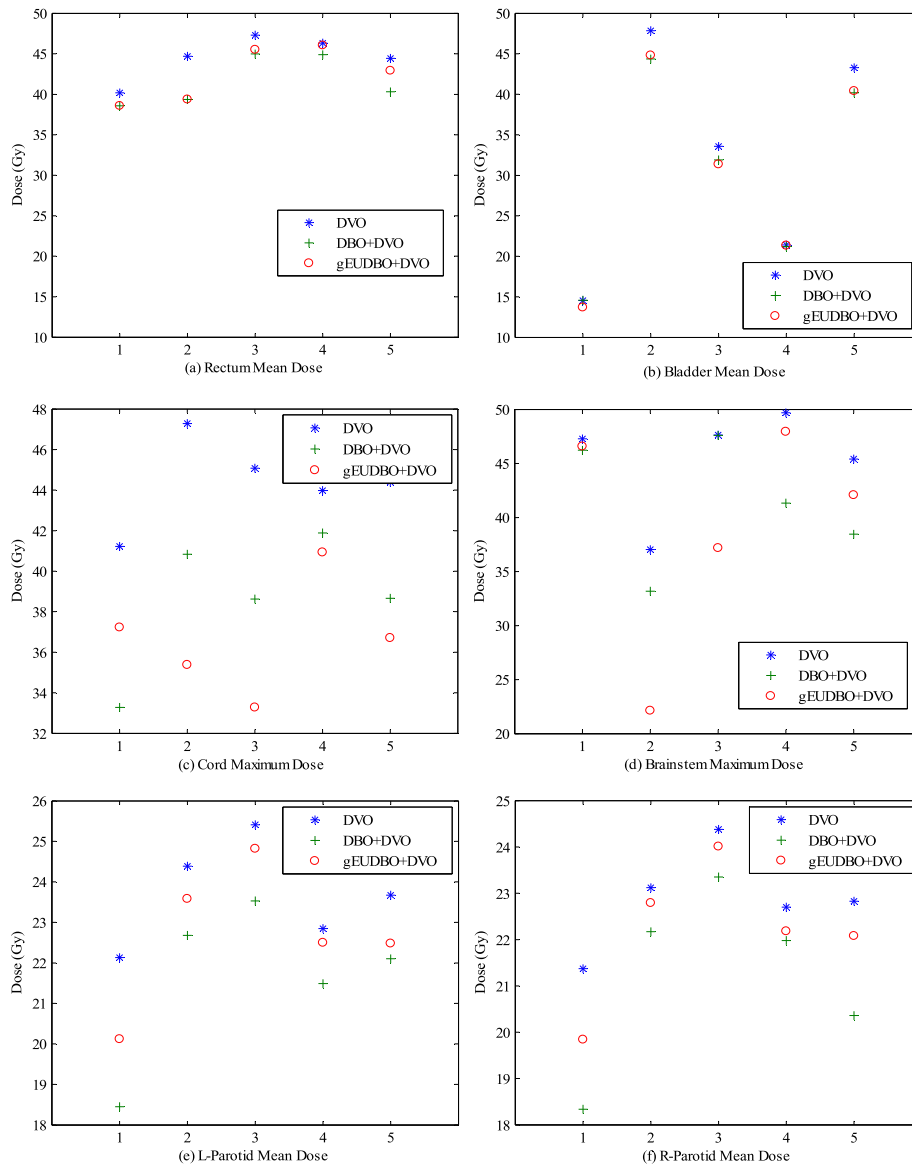
FIGURE 5. Comparative results of the OARs sparing. (a) rectum mean dose; (b) bladder mean dose; (c)cord maximum dose; (d) brainstem maximum dose; (e) L-Parotid mean dose; (f) R-Parotid mean dose. X- axis is the serial number for each cancer case.

cord and brainstem maximum doses, and the L-Parotid and R-Parotid mean doses were improved by 10.98%, 12.03%, 17.3%, 15.3%, 4.18%, and 3.06%, respectively. From the statistical analysis in Table 11, coverage and HI of all PTVs

in Fig. 4c and 4d appear to remain comparable in different plans.

From the above analyses, we conclude that the improved DVO plans yield better OAR-sparing achievement with
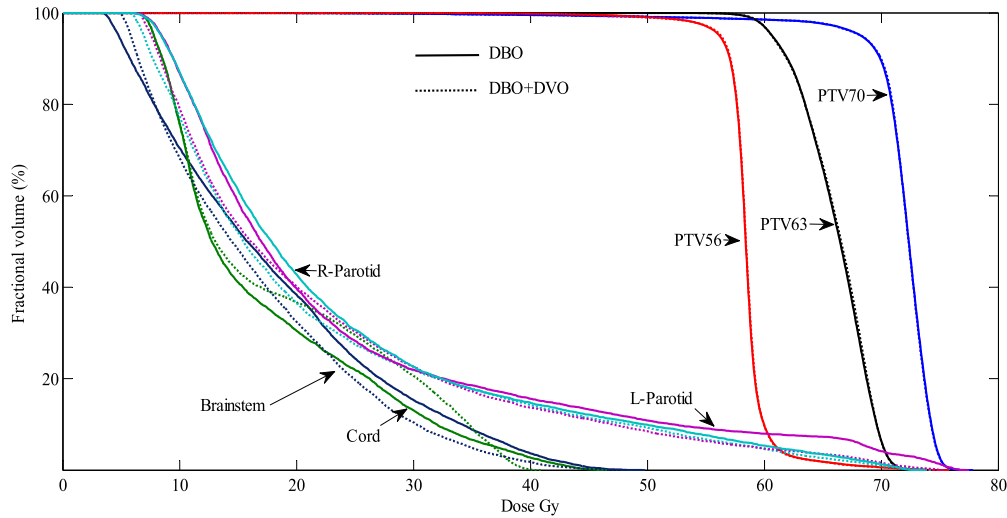
FIGURE 6. DVH comparison of one head and neck case. Solid line: DBO plan; Dotted line: DBO+DVO plan.

TABLE 10. Mean dose values of the plans in Fig. 4a and 4b using clinical metrics for prostate cancer.

Organ		Specific interest	DVO	DBO+DVO	gEUDBO+DVO
	PTV	V_{74} (%)	99.56±0.36	97.47±0.40	99.54±0.35
		V_{80} (%)	0	0	0
		HI	1.03±0.01	1.03±0.01	1.03±0.01
OARs	Rectum	V_{50} (%)	36.76±4.00	**32.60±4.45**	33.95±4.34
		V_{60} (%)	27.59±2.24	**25.22±2.44**	25.97±2.49
		V_{65} (%)	23.47±1.65	**21.94±1.71**	21.52±1.51
		V_{70} (%)	19.25±1.21	**18.50±1.22**	18.67±1.06
		V_{75} (%)	13.49±1.13	13.33±1.04	13.21±1.15
		V_{80} (%)	0	0	0
		D_{mean} (Gy)	44.60±2.74	**41.63±3.08**	42.49±3.42
	Bladder	V_{65} (%)	19.87±9.51	**18.73±8.35**	18.58±8.71
		V_{70} (%)	16.65±7.81	16.17±7.31	**16.02±7.60**
		V_{75} (%)	11.36±4.76	11.12±4.46	11.13±4.71
		V_{80} (%)	0	0	0
		D_{mean} (Gy)	32.13±14.12	30.45±12.50	30.33±12.94

TABLE 11. Mean dose values of the plans in Fig. 4c and 4d using clinical metrics for head-neck cancer.

Organ		Specific interest	DVO	DBO+DVO	gEUDBO+DVO
PTVs	PTV70	V_{70} (%)	95.32±3.60	94.93±3.85	94.68±3.48
		V_{77} (%)	0.78±0.61	0.74±0.63	0.74±0.70
		HI	1.08±0.01	1.07±0.02	1.07±0.01
	PTV63	V_{63} (%)	90.06±5.20	92.31±2.73	91.01±3.23
		$V_{67.4}$ (%)	42.16±2.23	33.32±6.35	37.53±6.48
		HI	1.13±0.02	1.12±0.01	1.13±0.02
	PTV56	V_{56} (%)	98.25±0.51	99.10±0.77	98.13±2.30
		$V_{59.9}$ (%)	9.57±3.26	9.02±4.61	8.42±2.71
		HI	1.08±0.01	1.08±0.02	1.07±0.01
OARs	Cord	V_{35} (%)	46.34±2.50	**1.69±1.71**	4.38±2.86
		D_{max} (Gy)	44.41±2.52	**38.67±3.83**	36.73±3.25
	Brainstem	V_{40} (%)	3.49±2.90	0.74±0.82	0.89±0.74
		D_{max} (Gy)	45.43±5.68	42.10±6.52	38.48±11.88
	L-Parotid	V_{50} (%)	11.2±0.68	9.31±0.52	10.3±0.88
		Dmean (Gy)	23.69±2.46	21.65±2.27	22.70±2.68
	R-Parotid	V_{50} (%)	9.71±1.65	**8.31±1.89**	8.52±2.12
		Dmean (Gy)	22.88±3.79	20.84±3.66	22.18±4.15

similar dose coverage for each target. The results of OARs sparing are presented in Fig. 5.a-Fig. 5.f for each cancer case. Those results are used to compare the DVO plan, DBO+DVO plan, and gEUDBO+DVO plan. It is obvious that solutions, calculated by the proposed DBO+DVO method and gEUDBO+DVO method, remarkably improved organ sparing.

The new DVO method was implemented in two steps. Next, we also investigated the difference between the plans obtained in the first step and the second step on all cases. Fig. 6 compares the DVHs of the DBO plan and the DBO+DVO plan on one head and neck cancer case and shows that the DVHs for critical structures in the DBO+DVO

TABLE 12. DV constraints of OARs for prostate cancer.

Organ	Parameters of DV constraints				
Bladder		V_{65}<50 %	V_{70}<35 %	V_{75}<25 %	V_{80}<15 %
Rectum	V_{50}<50%	V_{60} <35%	V_{65}<25%	V_{70}<20%	V_{75}<15%

plan have been improved, while the enhancements on all PTVs remain the same. Fig. 7 shows the differences between the gEUDBO plan and the gEUDBO+DVO plan on one prostate cancer case. It demonstrates better trade-off between the PTV coverage and the OARs sparing.
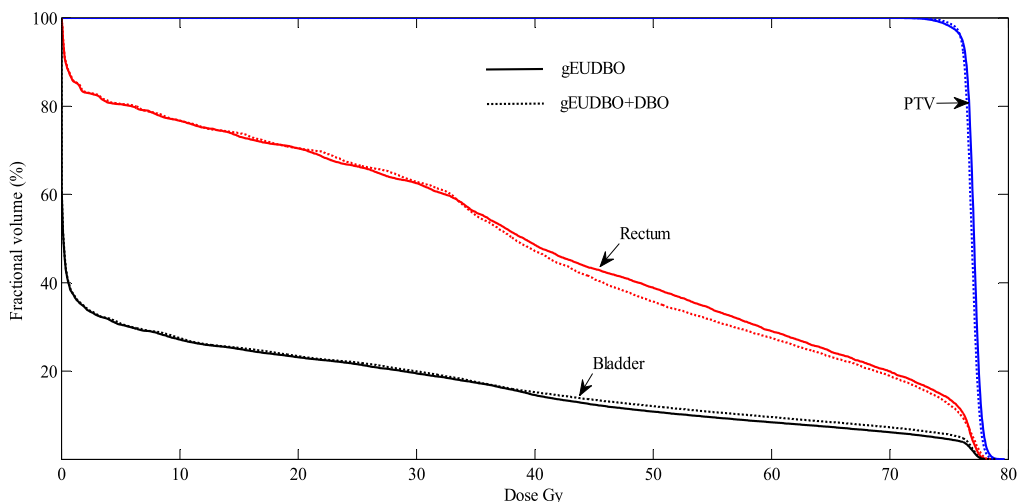
FIGURE 7. DVH comparison of one prostate case. Solid line: gEUDBO plan; Dotted line: gEUDBO+DVO plan.

TABLE 13. Number of iterations, computation times for the traditional DVO plan and the improved DVO plans.

Case		DVO	DBO+DVO	gEUDBO+DVO
prostate	No.iterations	31	26	28
	Time(s)	52	31	36
HN	No.iterations	60	30	40
	Time(s)	328	263	296

IV. DISCUSSIONS AND CONCLUSIONS

An efficient method to improve the quality of DVO treatment plan was successfully developed. Promising results were obtained in five prostate cases and five HN cases in terms of PTV coverage and OAR protection. Statistical data from our study demonstrated that our proposed DVO method yielded more satisfactory treatment plans than the plans generated by conventional DVO and the plans generated by optimization based on only organ model.

The improvements derived by using proposed increasing objective functions, may be attributed to the fact that the optimization algorithm has the capability to reduce doses either higher or lower than the prescribed doses to OARs, without sacrificing other optimization objectives. Thus, the search space is expanded. It should be noted that, in addition to linear term, we added other terms in the original physical-dose-based model and gEUD-based model to solve the problem of semi-deviation. For example, a quadratic term was added in the original organ-based-models. Through a series of experiments, we observed that the performance obtained by adding linear term is better than that by adding other term. The reason behind it needs to be further investigated.

Although our proposed DVO method, which needs the guide from organ-model-based optimization, appears to have increased complexity of DVO, the number of iterations and optimization time of DVO were actually reduced, as seen in

Table 13. The overall quality of improved DVO plans was improved. These improvements can be attributed to the initial intensity distributions for DVO.

In our study, we used the pencil beam dose calculation in CERR, but with different dose calculation methods such as modern superposition/convolution dose calculations. In most of the commercial planning systems, the AAA dose calculation was performed in Eclipse. However, this difference would not affect our conclusions drawn from the present study, because our study aimed to investigate the impact of optimized objective function on the search ability of optimization algorithm, which was not affected by dose calculation methods.

There are substantial differences between the method proposed by Wu *et al* [31] and our method. In Wu's method, the aim was to exploit the advantages of both systems by combining the gEUD-based and DV-based optimization methods together. Our aim was to develop an efficient method to determine more effective initial intensity distributions in X_{DVH} for DVO, in order to improve the quality of the DVO plan. Meanwhile, the minimum local error introduced by the non-convexity of dose-volume objective was simultaneously reduced.

For most testing cases, we found that the DBO+DVO plan was slightly better than the gEUD+DVO plan in terms of OARs sparing, with similar PTV coverage. The improvement may result from the fact that the improved physical-dosed-based increasing model directly gives the linear or quadratic penalty to each voxel in the optimized organ, according to the difference between actual dose and prescribed dose to each voxel. By contrast, the improved gEUD-based model, through comparing the calculated gEUD with prescribed $gEUD_0$, gives different degrees of linear penalty to the calculated gEUD. When $gEUD < gEUD_0$ or $gEUD > gEUD_0$, the voxels with higher dose or lower dose in optimized organ are given the same degree of penalty, which is not beneficial

to OAR sparing. Compared with the improved gEUD-based organ model, the merit of improved dose-based organ model has been verified in Fig. 3.

The gEUDBO+DVO plan shows improved OARs protection with similar PTV coverage compared to the DVO plan. At present, however, the biological optimization has increasing interests in radiotherapy research. In our proposed gEUDBO+DVO method, the biologically relevant optimization is firstly performed, followed by physical optimization. There are two reasons that accounts for this procedure. First, biological optimization has not been widely used due to the uncertainties associated with biological-based optimization models. Moreover, our proposed gEUDBO+DVO plan does not completely neglect biological optimization information from gEUD-based optimization (gEUDBO).

The initial intensity distributions from the organ-model-based optimization belong to random intensity distributions by nature. However, it is very difficult to generate the same random initial intensity distributions by the random methods. In other words, we proposed a more efficient method, compared to random method, to generate random initial intensity distributions for DVO, which can improve the planning quality.

Our proposed DVO method will also be beneficial to biological radiotherapy optimization as described by Das [2], who performed biological optimization after DVO. This method can improve the dose distribution without intentionally changing the optimization results achieved by DVO. For example, we can first use our proposed DBO+DVO method to generate a DVO plan, and then perform the DVO-guided biological optimization. How to change the quality of biological optimization plan via improving the quality of DVO remains uncertain, and this is one of our future research directions. In addition, improved DVO plan is also helpful to automatic re-optimization processes, as proposed by Li *et al.* [41] and Zarepisheh *et al.* [42]. Moreover, the improved increasing sub-scores, owing to their ability to enlarge the search solution space, will be beneficial to direct aperture optimization (DAO) [43]. The benefits will be verified in our thereafter works.

ACKNOWLEDGMENT

REFERENCES

[1] G. Kalantzis and A. Apte, "A novel reduced-order prioritized optimization method for radiation therapy treatment planning," *IEEE. Trans. Biomed. Eng.*, vol. 61, no. 4, pp. 1062–1070, Apr. 2014.

[2] S. Das, "A role for biological optimization within the current treatment planning paradigm," *Med. Phys.*, vol. 36, no. 10, pp. 4672–4682, 2009.

[3] J. O. Deasy, C. S. Mayo, and C. G. Orton, "Treatment planning evaluation and optimization should be biologically and not dose/volume based," *Med. Phys.*, vol.42. no. 6, pp. 2753–2756, 2015.

[4] D. Hristov, P. Stavrev, E. Sham, and B. G. Fallone, "On the implementation of dose-volume objectives in gradient algorithms for inverse treatment planning," *Med. Phys.*, vol. 29, no. 5, pp. 848–856, 2002.

[5] M. L. Hernando *et al.*, "Radiation-induced pulmonary toxicity: A dose-volume histogram analysis in 201 patients with lung cancer," *Int. J. Radiat. Oncol. Biol. Phys.*, vol. 51, pp. 650–659, Nov. 2001.

[6] S. L. S. Kwa *et al.*, "Evaluation of two dose–volume histogram reduction models for the prediction of radiation pneumonitis," *Radiotherapy Oncol.*, vol. 48, pp. 61–69, Jul. 1998.

[7] M. V. Graham *et al.*, "Clinical dose–volume histogram analysis for pneumonitis after 3D treatment for non-small cell lung cancer (NSCLC)," *Int. J. Radiat. Oncol. Biol. Phys.*, vol. 45, pp. 323–329, Sep. 1999.

[8] J. Miller, M. Fuller, S. Vinod, N. Suchowerska, and L. Holloway, "The significance of the choice of radiobiological (NTCP) models in treatment plan objective functions," *Austral. Phys. Eng. Sci. Med.*, vol. 32, no. 2, pp. 81–87, 2009.

[9] X. Zhang, H. Liu, X. Wang, L. Dong, Q. Wu, and R. Mohan, "Speed and convergence properties of gradient algorithms for optimization of IMRT," *Med. Phys.*, vol. 31, no. 5, pp. 1141–1152, 2004.

[10] J. O. Deasy, "Multiple local minima in radiotherapy optimization problems with dose–volume constraints," *Med. Phys.*, vol. 24, no. 7, pp. 1157–1161, 1997.

[11] Q. Wu and R. Mohan, "Multiple local minima in IMRT optimization based on dose–volume criteria," *Med. Phys.*, vol. 29, no. 7, pp. 1514–1527, 2002.

[12] J. Llacer, J. O. Deasy, T. R. Bortfeld, T. D. Solberg, and C. Promberger, "Absence of multiple local minima effects in intensity modulated optimization with dose–volume constraints," *Phys. Med. Biol.*, vol. 48, no. 2, pp. 183–210, 2003.

[13] C. G. Rowbottom and S. Webb, "Configuration space analysis of common cost functions in radiotherapy beam-weight optimization algorithms," *Phys. Med. Biol.*, vol. 47, no. 1, pp. 65–77, 2002.

[14] R. Jeraj, C. Wu, and T. R. Mackie, "Optimizer convergence and local minima errors and their clinical importance," *Phys. Med. Biol.*, vol. 48, no. 17, pp. 2809–2827, 2003.

[15] M. Zarepisheh, A. F. Uribe-Sanchez, N. Li, X. Jia, and S. B. Jiang, "A multicriteria framework with voxel-dependent parameters for radiotherapy treatment plan optimization," *Med. Phys.*, vol. 41, no. 4, p. 041705, 2014.

[16] D. C. Liu and J. Nocedal, "On the limited memory BFGS method for large scale optimization," *Math. Program.*, vol. 45, no. 1, pp. 503–528, 1989.

[17] C. Cotrutz, M. Lahanas, C. Kappas, and D. Baltas, "A Multiobjective gradient-based dose optimization algorithm for external beam conformal radiotherapy," *Phys. Med. Biol.*, vol. 46, no. 8, pp. 2161–2175, 2001.

[18] M. M. Coselmon, J. M. Moran, J. D. Radawski, and B. A. Fraass, "Improving IMRT delivery efficiency using intensity limits during inverse planning," *Med. Phys.*, vol. 32, no. 5, pp. 1234–1245, 2005.

[19] B. Choi and J. O. Deasy, "The generalized equivalent uniform dose function as a basis for intensity-modulated treatment planning," *Phys. Med. Biol.*, vol. 47, no. 20, pp. 3579–3589, 2002.

[20] Q. Wu, R. Mohan, A. Niemierko, and R. Schmidt-Ullrich, "Optimization of intensity-modulated radiotherapy plans based on the equivalent uniform dose," *Int. J. Radiat. Oncol. Biol. Phys.*, vol. 52, no. 1, pp. 224–235, 2002.

[21] C. Thieke, T. Bortfeld, A. Niemierko, and S. Nill, "From physical dose constraints to equivalent uniform dose constraints in inverse radiotherapy planning," *Med. Phys.*, vol. 30, no. 9, pp. 2332–2339, 2003.

[22] X. S. Qi, V. A. Semenenko, and X. A. Li, "Improved critical structure sparing with biologically based IMRT optimization," *Med. Phys.*, vol. 36, no. 5, pp. 1790–1799, 2009.

[23] M. Hartmann and L. Bogner, "Investigation of intensity-modulated radiotherapy optimization with gEUD-based objectives by means of simulated annealing," *Med. Phys.*, vol. 35, no. 5, pp. 2041–2049, 2008.

[24] D. N. Mihailidis *et al.*, "Superiority of equivalent uniform dose (EUD)-based optimization for breast and chest wall," *Med. Dosimetry*, vol. 35, no. 1, pp. 67–76, 2010.

[25] C. Holdsworth, M. Kim, J. Liao, and M. H. Phillips, "A hierarchical evolutionary algorithm for multiobjective optimization in IMRT," *Med. Phys.*, vol. 37, no. 9, pp. 4986–4997, 2010.

[26] T. Dirscherl, J. Alvarez-Moret, and L. Bogner, "Advantage of biological over physical optimization in prostate cancer?" *Z. Med. Phys.*, vol. 21, no. 3, pp. 228–235, 2011.

[27] Q. Diot, B. Kavanagh, R. Timmerman, and M. Miften, "Biological-based optimization and volumetric modulated arc therapy delivery for stereotactic body radiation therapy," *Med. Phys.*, vol. 39, no. 1, pp. 237–245, 2012.

[28] T.-F. Lee *et al.*, "Dosimetric advantages of generalised equivalent uniform dose-based optimisation on dose–volume objectives in intensity-modulated radiotherapy planning for bilateral breast cancer," *Brit. J. Radiol.*, vol. 85, no. 1019, pp. 1499–1506, 2012.

[29] RaySearch Laboratories AB SS, ''Biological optimization using the equivalent uniform dose (EUD) in Pinnacle3,'' RaySearch Lab. AB, Stockholm, Sweden, White Paper WP-EUD rev.1,0310, 2003.

[30] A. Niemierko, ''A generalized concept of equivalent uniform dose,'' *Med. Phys.*, vol. 26, no. 6, p. 1100, 1999.

[31] Q. Wu, D. Djajaputra, Y. Wu, J. Zhou, H. H. Liu, and R. Mohan, ''Intensity-modulated radiotherapy optimization with gEUD-guided dose–volume objectives,'' *Phys. Med. Biol.*, vol. 48, no. 3, pp. 279–291, 2002.

[32] D. Craft, M. Bangert, T. Long, D. Papp, and J. Unkelbach, ''Shared data for intensity modulated radiation therapy (IMRT) optimization research: The CORT dataset,'' *GigaScience*, vol. 3, p. 37, Dec. 2014.

[33] E. Dale, T. P. Hellebust, A. Skjønsberg, T. Høgberg, and D. R. Olsen, ''Modeling normal tissue complication probability from repetitive computed tomography scans during fractionated high-dose-rate brachytherapy and external beam radiotherapy of the uterine cervix,'' *Int. J. Radiat. Oncol. Biol. Phys.*, vol. 47, no. 4, pp. 963–971, 2000.

[34] S. T. H. Peeters, M. S. Hoogeman, W. D. Heemsbergen, A. A. M. Hart, P. C. M. Koper, and J. V. Lebesque, ''Rectal bleeding, fecal incontinence, and high stool frequency after conformal radiotherapy for prostate cancer: Normal tissue complication probability modeling,'' *Int. J. Radiat. Oncol. Biol. Phys.*, vol. 66, no. 1, pp. 11–19, 2006.

[35] E. B. Butler *et al.*, ''Smart (simultaneous modulated accelerated radiation therapy) boost: A new accelerated fractionation schedule for the treatment of head and neck cancer with intensity modulated radiotherapy,'' *Int. J. Radiat. Oncol. Biol. Phys.*, vol. 45, no. 1, pp. 21–32, 1999.

[36] J. O. Deasy, A. I. Blanco, and V. H. Clark, ''CERR: A computational environment for radiotherapy research,'' *Med. Phys.*, vol. 30, no. 5, pp. 979–985, 2003.

[37] H. Ren, Y. Lan, C. Li, X. Zhao, and Z. Min, ''A novel method for fluence map optimization with dose volume constraints in IMRT,'' in *Applied Informatics and Communication* (Communications in Computer and Information Science), vol. 224, D. H. Zeng, Ed. Berlin, Germany: Springer, Aug. 2011, pp. 582–589.

[38] A. Ahnesjö, M. Saxner, and A. Trepp, ''A pencil beam model for photon dose calculation,'' *Med. Phys.*, vol. 19, no. 2, pp. 263–273, 1992.

[39] X. Wang *et al.*, ''Effectiveness of noncoplanar IMRT planning using a parallelized multiresolution beam angle optimization method for paranasal sinus carcinoma,'' *Int. J. Radiat. Oncol. Biol. Phys.*, vol. 63, no. 2, pp. 594–601, 2005.

[40] L. B. Marks *et al.*, ''Use of normal tissue complication probability models in the clinic,'' *Int. J. Radiat. Oncol. Biol. Phys.*, vol. 76, no. 3, pp. S10–S19, 2010.

[41] N. Li *et al.*, ''Automatic treatment plan re-optimization for adaptive radiotherapy guided with the initial plan DVHs,'' *Phys. Med. Biol.*, vol. 58, no. 24, pp. 8725–8738, 2013.

[42] M. Zarepisheh *et al.*, ''A DVH-guided IMRT optimization algorithm for automatic treatment planning and adaptive radiotherapy replanning,'' *Med. Phys.*, vol. 41, no. 6, pp. 016711-1–016711-14, 2014.

[43] D. M. Shepard, M. A. Earl, X. A. Li, S. Naqvi, and C. Yu, ''Direct aperture optimization: A turnkey solution for step-and-shoot IMRT,'' *Med. Phys.*, vol. 29, no. 6, pp. 1007–1018, 2002.

CAIPING GUO received the M.S. degree in signal and information processing from the North University of China, China, in 2009. She is currently a Lecturer with the College of Taiyuan, Institute of Technology. She is currently pursuing the Ph.D. degree with the North University of China.

Her research interest is mainly in the area of signal processing and radiotherapy optimization.
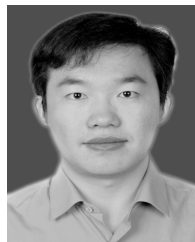
PENGCHENG ZHANG received the B.E. and M.E. degrees in signal and information processing from the North University of China, China, in 2006 and 2009, respectively, and the double Ph.D. degree in computer science and technology from the Université de Rennes and Southeast University in 2014.

He is currently with the School of Information and Communication Engineering, North University of China. His research interests include signal processing, CT reconstruction, and radiotherapy optimization.

ZHIGUO GUI received the Ph.D. degree in signal and information processing from the North University Of China, China, in 2004. He is currently a Professor with the North University of China.

His research interests include signal and information processing, image processing and recognition, and image reconstruction.

HUAZHONG SHU (M'00–SM'06) received the B.S. degree in applied mathematics from Wuhan University, Hubei, China, in 1987, and the Ph.D. degree in numerical analysis from the University of Rennes, France, in 1992.

He is currently a Professor with the Department of Computer Science and Engineering, Southeast University, Jiangsu, China. His recent work concentrates on the image analysis, pattern recognition, radiotherapy optimization, and fast algorithms of digital signal processing.

• • •